

SUPPLEMENTARY INFORMATION

Imaging of voltage-controlled switching of magnetization in highly magnetostrictive epitaxial Fe-Ga microstructures

Maite Goiriena,^{*a,b} Zhuyun Xiao,^{c,d} Rachel Steinhardt,^e Victor Estrada,^f Nobumichi Tamura,^d Rajesh V. Chopdekar,^d Alpha T. N'Diaye,^d Abdon Sepúlveda,^f Darrell G. Schlom,^{e,g} Rob N. Candler^{c,h} and Jeffrey Bokor^{a,i}

^a Department of Electrical Engineering and Computer Sciences, University of California, Berkeley, CA 94720, USA.

^b Department of Applied Physics, University of the Basque Country (UPV/EHU), 48013 Bilbao, Spain. E-mail: maite.goiriena@ehu.eus

^c Department of Electrical and Computer Engineering, University of California, Los Angeles, CA 90095, USA.

^d Advanced Light Source, Lawrence Berkeley National Lab, Berkeley, CA 94720, USA.

^e Department of Materials Science and Engineering, Cornell University, Ithaca, NY 14853, USA.

^f Mechanical and Aerospace Engineering Department, University of California, Los Angeles, CA 90095, USA.

^g Kavli Institute at Cornell for Nanoscale Science, Cornell University, Ithaca, NY 14853, USA.

^h California NanoSystems Institute, Los Angeles, CA 90095, USA.

ⁱ Materials Science Division, Lawrence Berkeley National Laboratory, Berkeley, CA 94720, USA.

Section 1. Crystallographic and magnetic characterization of the Fe-Ga thin film

Figure S1 presents the X-ray Φ scans of a 50 nm thick Fe-Ga film deposited on a (001)-oriented PMN-PT under conditions identical to those used for the 15 nm thick Fe-Ga described in the Experimental section. As depicted in Figure S1b, the 45° angular offset of the Fe-Ga (011) peaks relative to the PMN-PT (011) peaks reflects a 45° in-plane rotation of the Fe-Ga relative to the PMN-PT substrate. This orientation results in Fe-Ga [110] direction to align with the PMN-PT [100]. This finding, corroborated by the $\theta - 2\theta$ X-ray scan presented in the main manuscript (Figure 1a), further substantiates the single-crystal nature of the Fe-Ga thin film.

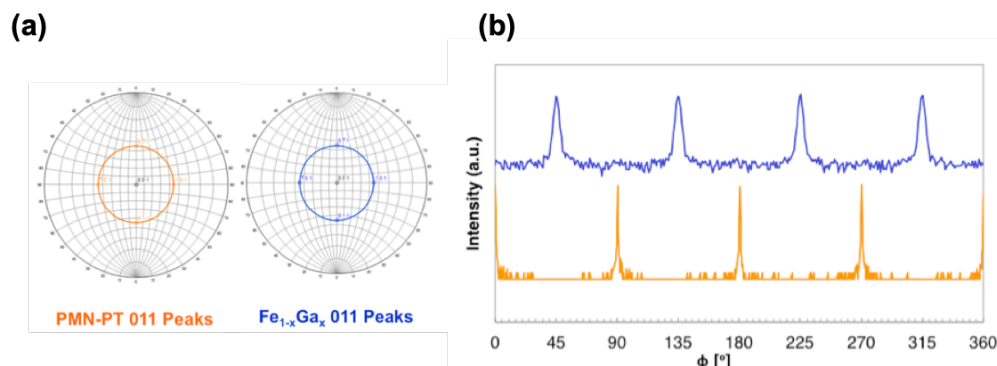


Figure S1. X-ray Φ scans of 50 nm Fe-Ga deposited on PMN-PT (001). (a) Stereographic projections for positions of the peaks in the scan. (b) PMN-PT 011 scan in orange and Fe-Ga 011 in blue.

Figure S2 illustrates the hysteresis loop of a 15 nm thick epitaxial Fe-Ga film on a (001)-oriented PMN-PT substrate, as measured by vibrating sample magnetometry (VSM). The applied magnetic field is aligned with the [100] direction of the PMN-PT, which is equivalent to the magnetic easy axis [110] of Fe-Ga film. The observed saturation magnetization, approximately 1100 kA m^{-1} , suggests that the Ga composition is close to 24%, in agreement with prior studies.^{1,2}

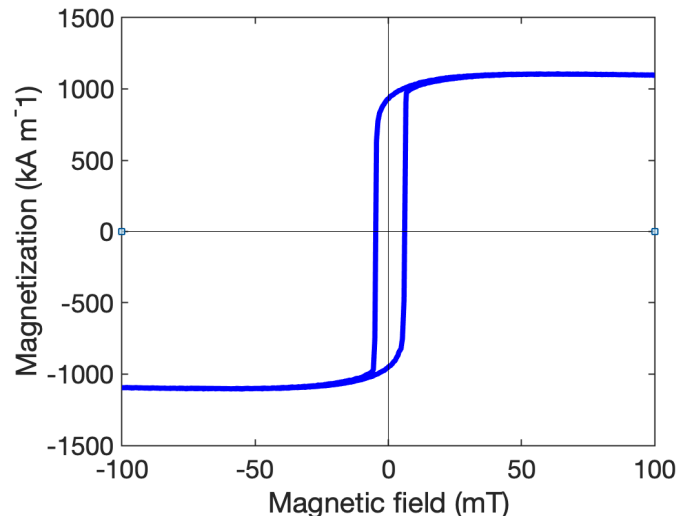


Figure S2. Vibrating sample magnetometry hysteresis loop for the epitaxial Fe-Ga thin film on (001)-oriented PMN-PT, measured along $[100]_p$, which is parallel to $[110]_{Fe}$.

X-ray magnetic circular dichroism (XMCD) offers additional insights into the element-specific magnetization characteristics. Figure S3 displays the X-ray absorption spectrum (XAS) and X-ray magnetic circular dichroism (XMCD) for Fe in a replicate PMN-PT/Fe/Fe-Ga/Pt sample, fabricated during the same growth cycle as the sample investigated in the main manuscript. To enhance the XMCD signal, the Pt capping layer was thinned from 4 nm to about 0.5 nm prior to measurement. The same etching process was also applied to the sample investigated in the manuscript prior to XMCD-PEEM. Notably, the remaining 0.5 nm Pt appears sufficient to shield the Fe-Ga thin film from oxidation, as evidenced by the lack of a shoulder-like peak feature around 706.9 eV, a signature typically associated with oxidized iron, in Figure S3a. These magnetic characterizations results underscore the high quality of the epitaxial Fe-Ga film developed on (001)-oriented PMN-PT.

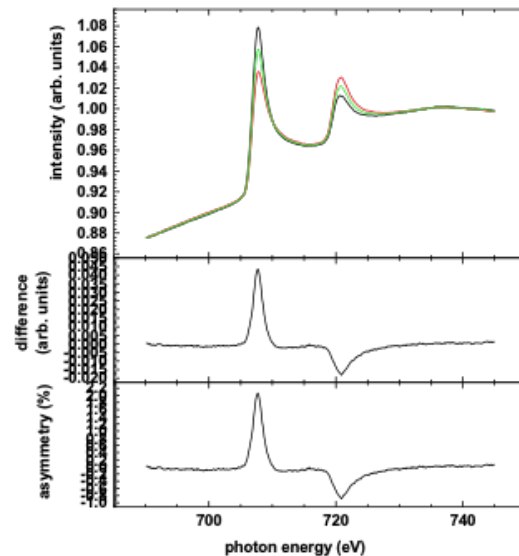


Figure S3. X-ray absorption spectra and X-ray magnetic circular dichroism of Fe L-2,3 edges.

Section 2. Stepwise voltage-induced reorientation of magnetization

Figure S4 presents a series of XMCD-PEEM images capturing the Fe-Ga microstructures' response under progressively increasing voltages. The images reveal that the switching field varies across different structures. For $1\ \mu\text{m}$ squares (Figure S4a), specifically for square number 2, vortex circulation reversal takes place somewhere in between $0.52\ \text{MV m}^{-1}$ and $0.76\ \text{MV m}^{-1}$. In the case of $2\ \mu\text{m}$ squares (Figure S4b), a domain wall displacement is already visible at $0.36\ \text{MV m}^{-1}$, which moves further away from the diagonal with increasing voltages. The image taken at $0.52\ \text{MV m}^{-1}$ has been left out of Figure S4 due to overexposure (the exposure time was too long), which obscures the distinction between actual magnetic domain configuration and artifacts. Thus, this image is deemed unsuitable for analyzing the magnetoelastic behavior of the $2\ \mu\text{m}$ squares. Finally, the voltage-induced switching in the ellipses is noted to occur between $0.36\ \text{MV m}^{-1}$ and $0.52\ \text{MV m}^{-1}$, as documented in Figure S4c.

Further insights from the XMCD-PEEM experiments indicate that the magnetoelectric actuation in the epitaxial Fe-Ga microstructures is non-volatile; the newly induced magnetic configurations persist even after the applied voltage is removed. This enduring response aligns the non-volatile, asymmetric *butterfly-like* loop behavior observed in the (001)-oriented PMN-PT.

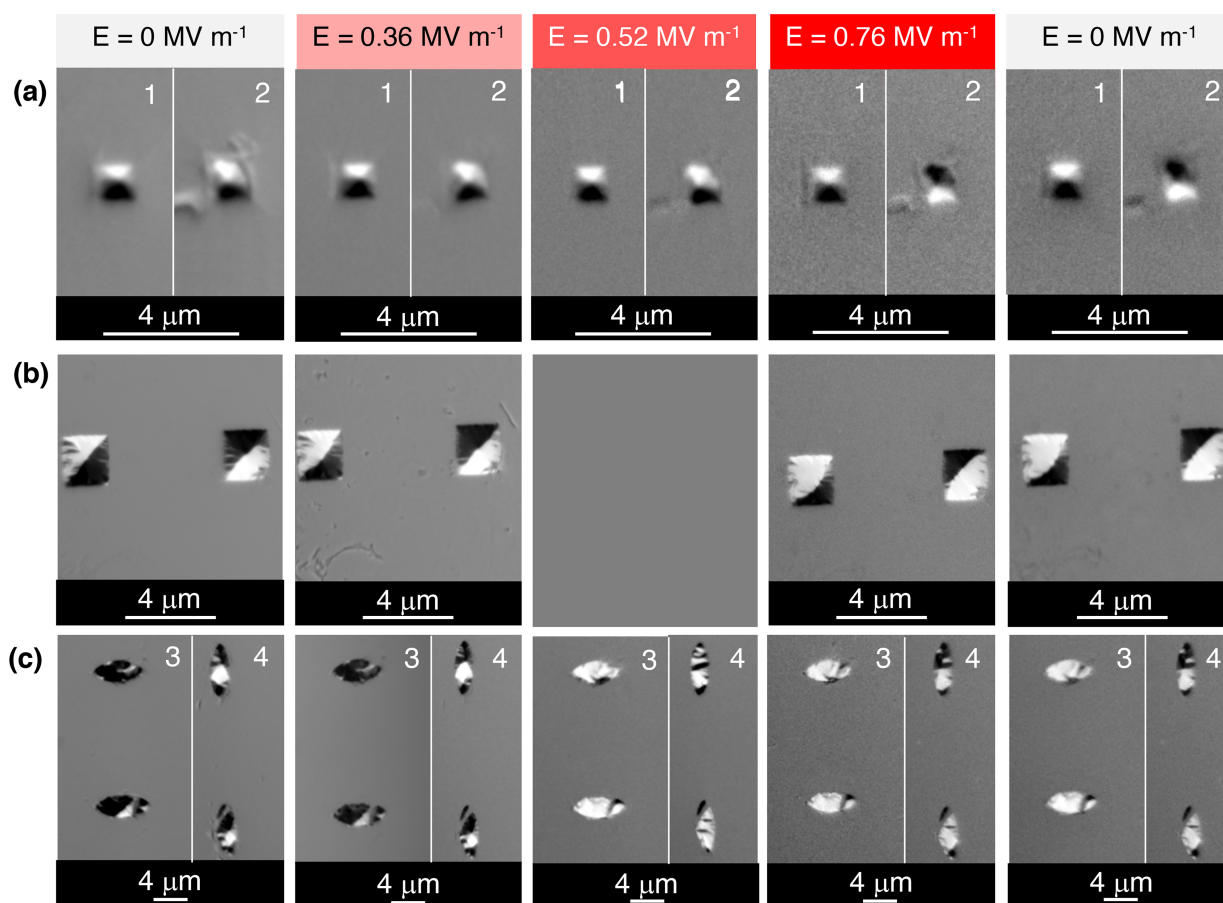


Figure S4. XMCD-PEEM images at Fe L_3 -edge showing the evolution of the magnetic configuration in epitaxial Fe-Ga microstructures at increasing applied voltages: (a) $1\ \mu\text{m}$ squares, (b) $2\ \mu\text{m}$ squares, (c-3) $6 \times 3\ \mu\text{m}^2$ ellipses aligned along $[100]_p$, and (c-4) $3 \times 6\ \mu\text{m}^2$ ellipses aligned along $[010]_p$. The last column shows the magnetic state when ramping down the voltage back to 0 V, showing non-volatile magnetic state.

Section 3. Quantitative analysis of the magnetic moment reorientation angle based on XMCD-PEEM images

To obtain the quantitative analysis of magnetic moment reorientation within the ellipses, we calculate and compare the magnetization angle in individual domains based on the contrast variations of the XMCD-PEEM images, following the calculation method reported by Z. Xiao *et al.*³

When the magnetic moment aligns parallel or anti-parallel to the X-ray propagation direction in-plane, the contrasts (C) are the strongest, and the magnetic moment direction would correspond to 0° or 180° . After subtracting the background ($C - C_{BG}$) in each XMCD-PEEM image at 0 MV m^{-1} , the strongest contrasts (C_{dark} and C_{light}) are observed in the $2 \mu\text{m}$ squares (Figure S5c). Next, these values are normalized through $C_N = (C - C_{MP}) / (C_{light} - C_{MP})$, where $C_{MP} = (C_{dark} + C_{light}) / 2$, resulting in -1 and 1 , and then converted into magnetic moment angle as $\cos^{-1}(C_N)$, giving 180° and 0° . The calculation is repeated in every distinguishable contrast area of the ellipses, which gives normalized values in between -1 and 1 , and magnetic moment angles in between 180° and 0° . The results are presented in Table S1, as well as in the magnetic domain maps in Figure S5a and S5b, where the arrows correspond to the calculated average magnetic angle. Different colors have been used to visualize the orientation of magnetization, representing an angle range of 0° - 75° (red), 75° - 105° (orange) or 105° - 180° (yellow). The orange arrows, being close to an angle of 90° (gray angle range in the color bar displayed in Figure S4c), can be pointing either up or down. Accordingly, the up or down direction has been used in the domain maps in Figure S5a and S5b to obtain a flux-closure magnetic configuration when possible, since it would be the most energetically favorable arrangement.

In order to calculate the voltage-induced rotation of the magnetization reported in the manuscript, we use the values of the magnetization direction of the largest domains for the ellipses aligned along $[100]_p$, and the values of the magnetization direction of the central domains for the ellipses aligned along $[010]_p$. The values are highlighted in Table S1.

Table S1. Quantification of magnetization direction in the magnetic domains in (a) ellipses with the long axis along $[100]_p$ and in (b) ellipses with the long axis along $[010]_p$. The angle of magnetization is the average angle \pm standard deviation of the magnetic moments in the domains marked by yellow (d), orange (g) and red (l) in Figure S5a and S5b. The highlighted values in (a) correspond to the largest magnetic domains and in (b) to the central magnetic domains, which are used to estimate the voltage-induced rotation of magnetization.

(a)	Magnetic domain at 0 MV m^{-1}	Angle of magnetization	Magnetic domain at 0.76 MV m^{-1}	Angle of magnetization	Rotation in major domain
Ellipse 1	l	$69^\circ \pm 7^\circ$	l	$59^\circ \pm 5^\circ$	$-92^\circ \pm 15^\circ$
	d	$151^\circ \pm 14^\circ$	g ₁	$91^\circ \pm 5^\circ$	
			g ₂	$99^\circ \pm 2^\circ$	
Ellipse 2	l ₁	$49^\circ \pm 11^\circ$	l ₁	$59^\circ \pm 7^\circ$	$-84^\circ \pm 18^\circ$
	l ₂	$63^\circ \pm 4^\circ$	l ₂	$60^\circ \pm 6^\circ$	
	g	$102^\circ \pm 4^\circ$	g	$87^\circ \pm 3^\circ$	
	d ₁	$143^\circ \pm 17^\circ$	d	$109^\circ \pm 4^\circ$	
	d ₂	$141^\circ \pm 12^\circ$			
Ellipse 3	l	$54^\circ \pm 6^\circ$	l	$60^\circ \pm 5^\circ$	$-83^\circ \pm 9^\circ$
	g	$105^\circ \pm 5^\circ$	d	$114^\circ \pm 3^\circ$	
	d ₁	$153^\circ \pm 6^\circ$			
	d ₂	$143^\circ \pm 8^\circ$			
Average rotation in major domain					$-86^\circ \pm 14^\circ$

(b)	Magnetic domain At 0 MV m^{-1}	Angle of magnetization	Magnetic domain at 0.76 MV m^{-1}	Angle of magnetization	Rotation in central domain
Ellipse 1	l	$32^\circ \pm 9^\circ$	l	$63^\circ \pm 6^\circ$	$31^\circ \pm 11^\circ$
	g ₁	$95^\circ \pm 16^\circ$	g ₁	$78^\circ \pm 5^\circ$	
	g ₂	$89^\circ \pm 9^\circ$	g ₂	$75^\circ \pm 3^\circ$	

	d_1	$128^\circ \pm 10^\circ$	d_1	$116^\circ \pm 7^\circ$	
	d_2	$137^\circ \pm 19^\circ$	d_2	$114^\circ \pm 5^\circ$	
Ellipse 2	l_1	$29^\circ \pm 12^\circ$	l_1	$69^\circ \pm 6^\circ$	$36^\circ \pm 13^\circ$
	l_2	$70^\circ \pm 11^\circ$	l_2	$65^\circ \pm 5^\circ$	
	g_1	$87^\circ \pm 18^\circ$	g_1	$94^\circ \pm 4^\circ$	
	g_2	$90^\circ \pm 11^\circ$	g_2	$99^\circ \pm 7^\circ$	
	d_1	$138^\circ \pm 11^\circ$	d	$114^\circ \pm 5^\circ$	
	d_2	$120^\circ \pm 9^\circ$			
Average rotation in central domain					$34^\circ \pm 12^\circ$

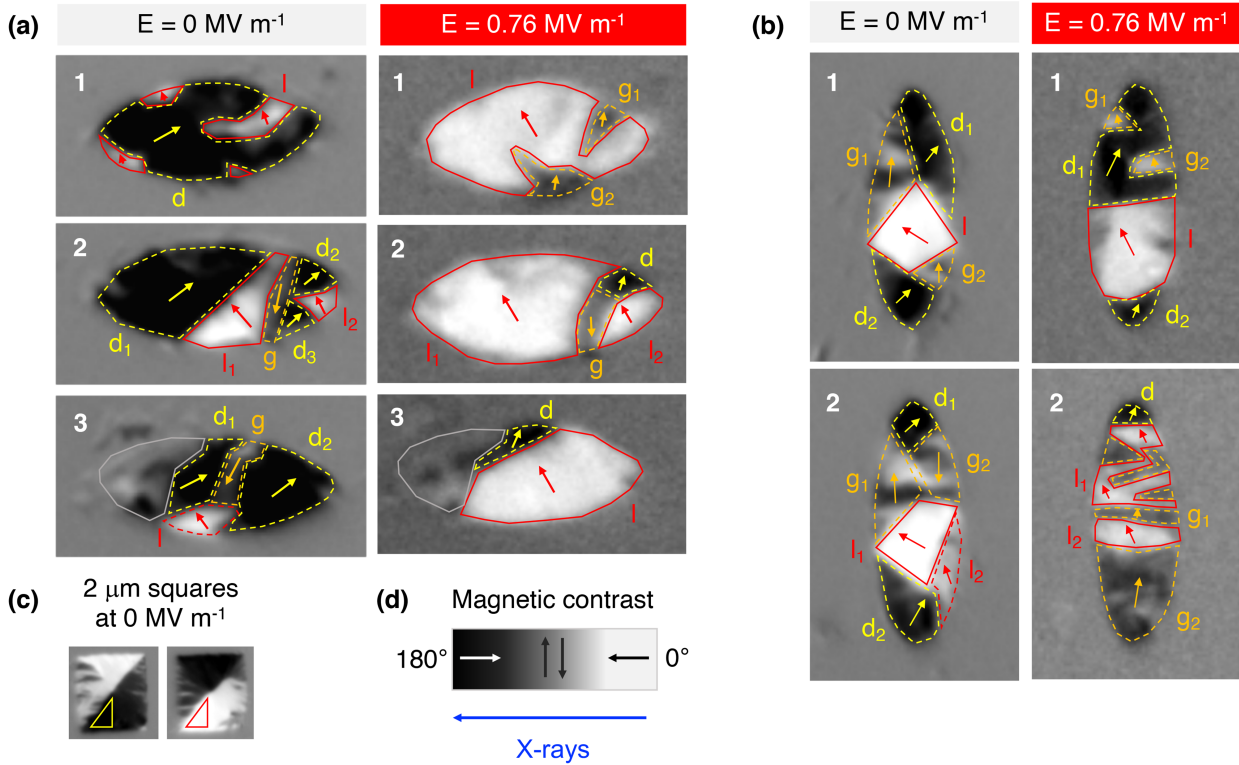


Figure S5. Magnetic domain maps of ellipses aligned along (a) $[100]_P$ and (b) $[010]_P$, where the average magnetization directions, calculated based on XMCD-PEEM images, are indicated by red (0° - 75°), orange (75° - 105°) and yellow (105° - 180°) arrows. (c) The strongest contrast values in $2 \mu\text{m}$ squares at 0 MV m^{-1} are used as C_{dark} and C_{light} in the calculations, leading to -1 (180°) and 1 (0°), respectively. (d) Gray scale bar describing the contrast levels of magnetic orientation with respect to the direction of the incident X-rays in the XMCD-PEEM images.

Section 4. Micromagnetic simulations of the magnetoelectric behavior

The material parameters used in the simulation are either taken from literature or measured directly: saturation magnetization $M_S = 1100 \text{ kA m}^{-1}$ (measured by VSM); strains along $[100]_P$ and along $[010]_P$, ε_{100} and ε_{010} (measured by X-ray microdiffraction, see Table S2); exchange stiffness constant $A_{ex} = 17 \times 10^{-12} \text{ J m}^{-1}$; damping constant $\alpha = 0.04$;⁴ magnetostriction constant $\lambda_{100} = 207 \times 10^{-6}$;¹ elastic constants $C_{11} = 205 \text{ GPa}$ and $C_{12} = 160 \text{ GPa}$,⁵ and cubic magnetocrystalline constants $K_1 = -1.2 \text{ kJ m}^{-3}$, $K_2 = 5 \text{ kJ m}^{-3}$.¹

Table S2. Average strain values along $[100]_p$ and $[010]_p$ at increasing voltages, measured by X-ray microdiffraction.

	$E = 0 \text{ MV m}^{-1}$	$E = 0.36 \text{ MV m}^{-1}$	$E = 0.52 \text{ MV m}^{-1}$	$E = 0.76 \text{ MV m}^{-1}$
ϵ_{100} (%)	-0.015	0.115	0.096	0.086
ϵ_{010} (%)	0.013	-0.009	-0.011	-0.025

First, the Fe-Ga microstructures are initialized to obtain the experimentally observed magnetic configurations at 0 MV m^{-1} , followed by applying two anisotropy terms: $K_{u1} = \frac{3}{2} \lambda_{100} \sigma_{100}$ and $K_{u2} = \frac{3}{2} \lambda_{100} \sigma_{010}$ to imitate the effect of the voltage-induced strain, where σ_{100} and σ_{010} are the stress values calculated as $\sigma_{100} = C_{11} \epsilon_{100} + C_{12} \epsilon_{010}$ and $\sigma_{010} = C_{12} \epsilon_{100} + C_{11} \epsilon_{010}$. The micromagnetic simulation results are shown in Figure S6a where each simulated configuration is compared to the corresponding XMCD-PEEM image at every applied voltage step. Figure S6b is a schematic description of the sample orientation in both the simulation and the experiments.

The $1 \mu\text{m}$ squares are initialized in the magnetic vortex state and then allowed to relax under the influence of its cubic magnetocrystalline anisotropy. With an applied electric field of 0.36 MV m^{-1} , the simulation shows an equal growth of both light and dark domains, corresponding to a parallel and an antiparallel magnetization direction with respect to the incident X-rays, aligned along the newly induced tensile strain. This is due to the inverse magnetostriction effect, which in the case of the positive magnetostrictive Fe-Ga, enhances the magnetic anisotropy along the tensile strain direction. It is possible that such change happens in the XMCD-PEEM experiment as well. However, it is hard to appreciate and quantify variations in domain size due to domain walls not being well defined. The vortex circulation reversal discussed in the manuscript is not reproduced by the model used here, though a similar behavior has been simulated elsewhere by applying a time-varying strain in $0.5 \mu\text{m}$ squares of epitaxial Fe-Ga.⁶

In order to initialize the $2 \mu\text{m}$ squares in a stable bidomain configuration, a uniaxial anisotropy term needs to be added along the square diagonal. As explained in the manuscript, a net uniaxial anisotropy may arise from fabrication-related strains or pre-existing non-uniform strain distribution in the PMN-PT substrate. While a uniaxial anisotropy of 5 kJ/m^3 is the minimal requirement to stabilize a bidomain state in our $2 \mu\text{m}$ epitaxial Fe-Ga squares, an anisotropy of 10 kJ/m^3 more accurately mimics the observed DW motion and curving under voltage application. However, as depicted in Figure S6a, the simulated DW exhibits more pronounced S-shaped curving compared to what is seen experimentally, likely due to the model considering only the uniaxial tensile strain effects. In experimental scenarios, the squares experience a non-uniform strain distribution that escalates with applied voltage, serving as the primary influence on DW dynamics rather than the uniform tensile anisotropy along $[100]_p$. This phenomenon has been corroborated by in the work of Lo Conte *et al.*⁷

The ellipse with the long axis along $[100]_p$, horizontally oriented in Figure S6a, is initialized as the experimental sample, *i.e.* by applying an external magnetic field (ramping up to 100 mT and down to 0 mT , with a step size of 2.5 mT). Additionally, the experimentally observed light-colored domains of this specific ellipse are manually included in the simulated model, which could be originated by pinning effects at structural imperfections. Moreover, these domains seem to play a key role in the voltage-induced magnetic reorientation, since they grow at the expense of the initially predominant dark-colored domain, favored by the newly induced tensile strain.

The ellipse with the long axis along $[010]_p$, vertically oriented in Figure S6a, is also initialized with an external magnetic field that is ramped up and down, as for the horizontal ellipse. This leads to a flux closure pattern similar to what observed experimentally, with a characteristic rectangular domain at the center. In the simulation, at 0.36 MV m^{-1} we observe a new configuration with three magnetic domains parallel to the voltage-induced tensile strain direction, due to the inverse magnetostrictive effect. In the experimental case, a similar reorientation of DWs occur somewhere in between 0.36 MV m^{-1} and 0.52 MV m^{-1} , showing a stripe-like domain configuration with the DWs also aligned along $[100]_p$. A possible explanation of the ellipse breaking into more than three domains is probably due to the more complex initial domain configuration and pinning and nucleation of magnetic domains, where we can already distinguish a stripe-like texture in some domains.

Finally, the switching field being lower in the simulation than in the experiment, is probably due to the more ideal conditions of the model, *e.g.*, pinning-free and heterogeneous strain-distribution. These factors lead to a simpler magnetoelastic effect with undisrupted DW motion and reorientation of magnetization. Remarkably, we show that by using the measured strains, the model reproduces the observed magnetoelectric switching events, in a qualitative fashion, confirming that the main driving force of the epitaxial Fe-Ga microstructures is voltage.

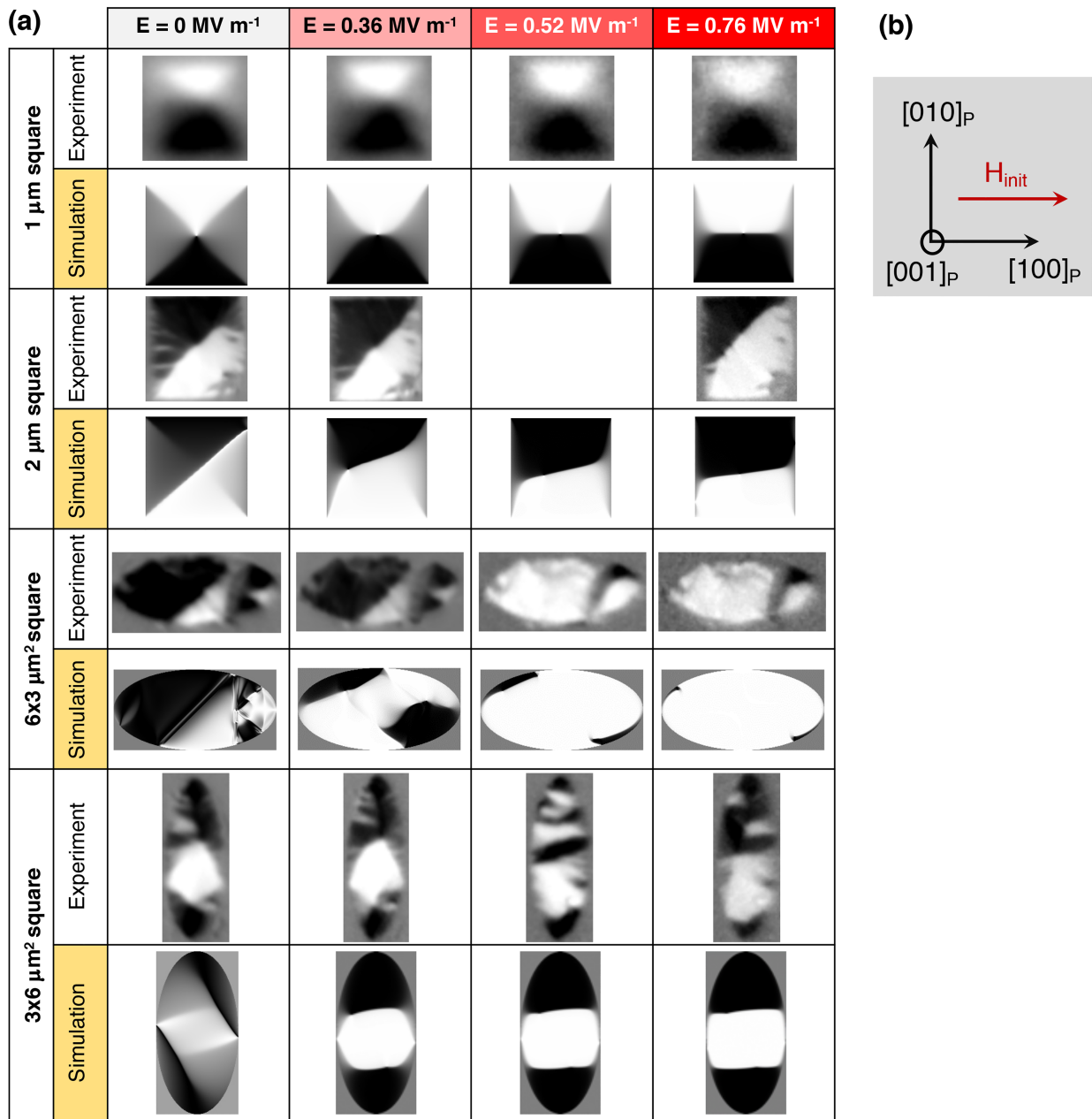


Figure S6. (a) Results of micromagnetic simulation outcomes for all investigated Fe-Ga microstructures, using experimentally measured strain values at each applied voltage, alongside typical material parameters for Fe-Ga reported in the existing research. (b) Schematic description of the sample orientation and applied fields in both the simulation and the experiments.

- 1 S. Datta, J. Atulasimha, C. Mudivarthi and A.B. Flatau, *J. Magn. Magn. Mater.* 2010, **322**, 2135.
- 2 A. E. Clark, K. B. Hathaway, M. Wun-Fogle, J. B. Restorff, Thomas A. Lograsso, V. M. Keppens, G. Petculescu and R. A. Taylor, *J. Appl. Phys.* 2003, **93**, 8621.
- 3 Z. Xiao, R. Lo Conte, M. Goiriena-Goikoetxea, R. V. Chopdekar, C.-H. A. Lambert, X. Li, A. T. N'Diaye, P. Shafer, S. Tiwari, A. Barra, A. Chavez, K. P. Mohanchandra, G. P. Carman, K. L. Wang, S. Salahuddin, E. Arenholz, J. Bokor and R. N. Candler, *ACS Appl. Mater. Interfaces* 2020, **12**, 6752.
- 4 D. B. Gopman, V. Sampath, H. Ahmad, S. Bandyopadhyay and J. Atulasimha, *IEEE Transactions on Magnetism* 2017, **53**, 1.

- 5 Y.-Ning Zhang, R.-Qian Wu, H. M. Schurter and A. B. Flatau, *Journal of Applied Physics* 2010, **108**, 023513.
- 6 T. A. Ostler, R. Cuadrado, R. W. Chantrell, A. W. Rushforth and S. A. Cavill, *Phys. Rev. Lett.* 2015, **115**, 067202.
- 7 R. Lo Conte, Z. Xiao, C. Chen, C. V. Stan, J. Gorchon, A. El-Ghazaly, M. E. Nowakowski, H. Sohn, A. Pattabi, A. Scholl, N. Tamura, A. Sepulveda, G. P. Carman, R. N. Candler and J. Bokor, *Nano Lett.* 2018, **18**, 1952.